Dalton Transactions

ROYAL SOCIETY OF CHEMISTRY

PAPER

View Article Online
View Journal | View Issue

Cite this: *Dalton Trans.*, 2024, **53**, 18304

Monolayers of a thiacalix[3]pyridine-supported molybdenum(0) tricarbonyl complex on Au(111): characterisation with surface spectroscopy and scanning tunneling microscopy†

Kai Uwe Clausen,[a] Xiangzhi Meng,[b] Katrin Reisig,[a] Christian Näther,[a] Thomas Strunskus,[c] Richard Berndt[b] and Felix Tuczek*[a]

Received 4th September 2024,
Accepted 21st October 2024

DOI: 10.1039/d4dt02521k

rsc.li/dalton

Deposition of dome-shaped metal–organic complexes on metallic surfaces to produce well-defined single site catalysts is a novel approach combining aspects of homogeneous and heterogeneous catalysis. In order to investigate the bonding of small molecules to such systems, a molybdenum(0) tricarbonyl complex supported by a thiacalix[3]pyridine is synthesized and deposited on Au(111) and Ag(111) surfaces by vacuum evaporation. The resulting mono- and submonolayers are investigated with surface spectroscopy and STM. All of these methods indicate a parallel orientation of the molybdenum complex with respect to the surface. The vibrational properties and frequency shifts of the adsorbed complexes with respect to the bulk are evaluated with the help of conventional IR and IRRA spectroscopy, coupled to DFT calculations. Compared to a similar Mo(0) tricarbonyl complex supported by an azacalixpyridine ligand, the title complex exhibits a higher stability in the bulk and adsorbed to surfaces which goes along with a lower reactivity towards oxygen.

Introduction

In order to solve the energy and environmental challenges our planet and humanity are facing today, new and alternative concepts in catalysis have to be explored. More than 90% of all industrial chemical processes involve catalytic steps whereby heterogeneous catalysis dominates with about 80%.[1,2] One challenge is to create such systems having well-defined (structurally identical) active sites with a high surface density.[3–7] An attractive approach towards that goal, pursued in the field of surface organometallic chemistry (SOMC) is to deposit metal–organic complexes (MOCs), possessing a single transition metal atom in a highly controlled ligand environment, on surfaces to produce single-site heterogeneous catalysts.[3–7]

In the literature MOCs have mainly been attached covalently (grafted) to surfaces by reaction of the oxo ligands with metal–oxide based supports such as SiO_2, MgO and others to guarantee strong anchoring of the transition metal to the surface.[3–7] Alternatively, metal–organic molecules have been physisorbed to noble metal surfaces (Cu, Ag, Au).[8–13] In this regard, porphyrins and phthalocyanines which form highly stable complexes and have important functions and applications, are the best studied systems so far.[14] However, porphyrinoid macrocycles show a reduced reactivity towards gaseous molecules when adsorbed on surfaces. Due to their flat geometry, the coordinated transition-metal centers are located very close to the surface. This results in a strong interaction with the underlying substrate, weakening the bonding of small molecules in trans-position; *i.e.*, towards the gas phase ("surface trans-effect").[11,12,15]

One way to reduce the contact between the central atom of the MOC and the surface and thus mitigate the surface trans-effect (while still maintaining some electronic interaction) is to diminish the size of the ring. The smaller cavity compared to porphyrins and phthalocyanines lifts the metal center above the ligand plane and thus increases its distance to the surface. In the corresponding dome-shaped complexes, the interaction with the underlying surface is reduced, which should allow binding and eventual catalytic conversion of molecules from the gas phase (Fig. 1). For this purpose subporphyrins, triphyrins, subphthalocyanines and other contracted macrocycles are suitable ligands.[8–10,16]

[a]*Institute of Inorganic Chemistry, Christian-Albrechts-University of Kiel, Max-Eyth-Straße 2, 24118 Kiel, Germany. E-mail: ftuczek@ac.uni-kiel.de*
[b]*Institute of Experimental and Applied Physics, Christian-Albrechts-University of Kiel, Leibnizstraße 11-19, 24118 Kiel, Germany*
[c]*Department of Material Science, Christian-Albrechts-University of Kiel, Kaiserstraße 1, 24118 Kiel, Germany*

†Electronic supplementary information (ESI) available. CCDC 2366199. For ESI and crystallographic data in CIF or other electronic format see DOI: https://doi.org/10.1039/d4dt02521k

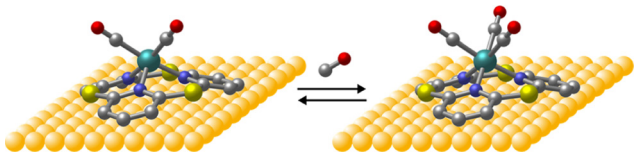

Fig. 1 Concept of a hybrid catalytic system by deposition dome-shaped metal–organic complexes (MOCs) on metal surfaces providing the opportunity to bind and catalytically convert molecules from the gas phase. (Shown are DFT optimized gas phase structures positioned on a surface).

Notably the metal substrate not only exerts an electronic influence on the MOC, but can also activate and orient adsorbed reactants of the catalytic reaction itself.[1,17] If the reactive properties of the substrate are taken into account, the assembly of MOCs on metallic surfaces potentially leads to hybrid catalytic systems (*cf.* Fig. 1). Their physicochemical properties can be modified in four ways: (1) by choosing different metal surfaces, (2) incorporating different transition metals into the MOCs, (3) tuning the electronic structure of the ligand and (4) modifying the distance between the metal center of the MOC and the underlying substrate through variation of the ring size of the supporting macrocycle.

Recently, we reported on a molybdenum(0) tricarbonyl complex supported by *N*-(*p*-tolyl)azacalix[3](2,6)-pyridine. This compound reacts with molecular oxygen (O_2) in solution, in the bulk and with surface-adsorbed monolayers to form the corresponding molybdenum(VI) trioxo complex, which in turn catalytically mediates oxygen transfer.[8,9] However, due to the additional tolyl groups in the azacalixpyridine ligand being oriented perpendicularly to the plane through the three pyridine nitrogen atoms,[8,18] the complex molecules were found to be adsorbed in a slightly tilted orientation with respect to the surface normal. We therefore decided to explore the properties of molybdenum tricarbonyl complexes supported by thiacalixpyridine ligands which do not possess substituents at the atoms bridging the pyridine moieties. However, this modification expands the cavity of the macrocycle and possibly also influences the electronic and geometric structure of the corresponding carbonyl complex.

The tridentate macrocycle thiacalix[3](2,6)pyridine (**2**) (Py_3S_3) and the derived molybdenum(0) tricarbonyl complex **1** are shown in Scheme 1. Herein, complex **1** is investigated in the solid state, in homogenous solution and adsorbed on noble metal surfaces (Ag, Au) employing a range of spectroscopic and analytical methods to elucidate its electronic structure and the adsorption geometry on Au(111) and Ag(111) as well as assess the reactive potential of the resulting metal surface/metal–organic complex (MOC) hybrid systems.

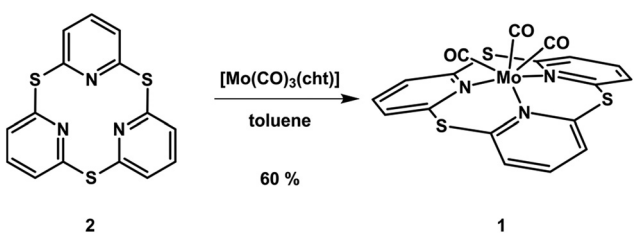

2 1

Scheme 1 Synthesis of the complex $[Mo(CO)_3(Py_3S_3)]$ (**1**).

Results and discussion

Synthesis and characterization of $[Mo(CO)_3(Py_3S_3)]$ (1) in solution and the solid state

For the synthesis of the dome shaped complex **1** the thiacalix[3]pyridine ligand (Py_3S_3) (**2**) was chosen. This ligand was prepared in analogy to the literature in a one step synthesis using 2,6-dibromopyridine and sodium hydrogensulfide (for more details see ESI Chapter 2†).[19] Reaction of ligand **2** with the precursor complex [Mo(CO)$_3$(cycloheptatriene)] in toluene afforded the molybdenum(0) tricarbonyl complex $[Mo(CO)_3(Py_3S_3)]$ (**1**) in 60% yield (see Scheme 1).

Crystals of **1**·0.5 DMSO suitable for single crystal X-ray determination were obtained by slow diffusion of diethylether into a solution of **1** in dimethyl sulfoxide (DMSO) under argon atmosphere. The structure of the molybdenum(0) tricarbonyl complex **1** is shown in Fig. 2. Selected bond distances and angles are collected in Table 1 (see also ESI Chapter 4†).

Complex **1** exhibits a slightly trigonally distorted octahedral coordination around the Mo(0) center with two opposite trigonal faces being occupied by the three pyridyl nitrogen atoms and three carbonyl ligands, respectively. The average angles between the C–Mo–C-atoms (84.67°) and the carbonyl C- and the trans pyridine N-atom (176.96°) are in agreement with those related structures reported in the literature and are characteristic of $Mo(CO)_3$ complexes with tridentate N-donor ligands.[8,20–27] However, in comparison with other Mo(0) tricarbonyl complexes supported by cyclic tridentate ligands such as tach,[24] tacn[25,26] TAM[27] and azacalixpyridine[8] the N–Mo–N angle (80.92°) in **1** is higher; actually it is the highest value reported for this type of complex so far. The reason for this

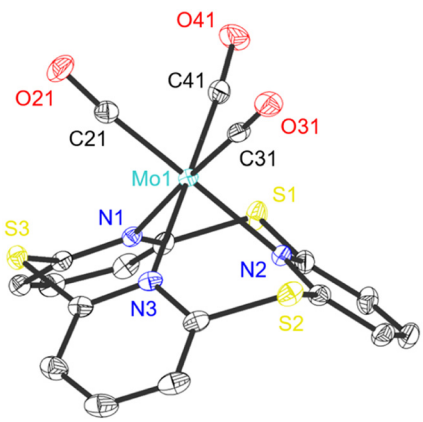

Fig. 2 ORTEP plot of complex $[Mo(CO)_3(Py_3S_3)]$ (**1**) with labelling and displacement ellipsoids drawn at the 30% probability level.

Table 1 Selected bond lengths [Å] and angles [°] of $[Mo(CO)_3(Py_3S_3)]$ (**1**)

Mo(1)–C(21)	1.9471(19)	N(1)–Mo(1)–C(41)	96.15(6)
Mo(1)–C(31)	1.9470(19)	N(2)–Mo(1)–C(31)	96.57(6)
Mo(1)–C(41)	1.9381(19)	N(2)–Mo(1)–C(41)	98.09(6)
Mo(1)–N(1)	2.2736(14)	N(3)–Mo(1)–C(21)	99.43(6)
Mo(1)–N(2)	2.2826(14)	N(3)–Mo(1)–C(31)	96.41(6)
Mo(1)–N(3)	2.2760(14)	C(21)–Mo(1)–C(31)	86.06(7)
O(21)–C(21)	1.164(2)	C(21)–Mo(1)–C(41)	81.43(7)
O(31)–C(31)	1.168(2)	C(31)–Mo(1)–C(41)	86.51(8)
O(41)–C(41)	1.168(2)	Mo(1)–C(21)–O(21)	174.67(16)
		Mo(1)–C(31)–O(31)	178.56(16)
N(1)–Mo(1)–C(31)	176.57(6)	Mo(1)–C(41)–O(41)	175.29(7)
N(2)–Mo(1)–C(21)	177.30(6)	N(1)–Mo(1)–N(2)	80.93(5)
N(3)–Mo(1)–C(41)	177.00(6)	N(1)–Mo(1)–N(3)	80.90(5)
N(1)–Mo(1)–C(21)	96.47(6)	N(2)–Mo(1)–N(3)	80.92(5)

observation lies in the fact that, due to the bridging sulfur atoms, the cavity of ligand **2** is significantly larger than in the other cyclic tridentate ligands, resulting in a less trigonally elongated and, thus, more regular octahedral coordination.

The molybdenum(0) carbonyl complex **1** was also spectroscopically characterized in solution and in the bulk. The NMR spectra (^{1}H and ^{13}C NMR) are shown in Fig. S1 and S2.† All resonances could be assigned to the respective carbon atoms by using the 2D correlation NMR techniques and DEPT-135-spectroscopy. Hereby, the signal of the CO ligands are of particular interest. Due the approximate C_{3v} symmetry of the complex (actually C_s) only a single signal is expected in the ^{13}C NMR and in fact only a singlet at 232.7 ppm is observed in the typical spectral range for CO ligands.

Complex **1** was further investigated by infrared and Raman spectroscopy. Vibrational spectroscopy is generally useful for monitoring the activation of small molecules such as the carbonyl ligands when coordinated to transition metal centers.[8,28,29] The IR (top) and Raman (bottom) spectra of **1** are shown in Fig. 3. From a spectroscopic point of view the complex can be assigned to the symmetry C_s. As expected for this point group three CO bands are observable both in the IR and in the Raman spectra.[30] The totally symmetric A′(1) vibration, in which all carbonyl ligands oscillate in phase, is located at 1888 cm^{-1} (Fig. 3 red). A second A′ vibration mode (A′(2)) is located at 1782 cm^{-1}. This vibration overlaps due to the approximate C_{3v} symmetry with the A″ vibrational mode at 1761 cm^{-1}. Hereby, the relative intensity of the A″ mode dominates in the IR and that of the A′(2) vibration in the Raman spectrum. Taken together, the results of the vibrational spectroscopy indicate a strong activation of the carbonyl ligands compared to free carbon monoxide (2143 cm^{-1}),[31] in agreement with the previously reported azacalixpyridine-supported complex (1893 cm^{-1}, 1768 cm^{-1} and 1750 cm^{-1})[8] and other molybdenum(0) tricarbonyl complexes with N-donor ligands.[8,20–27]

Deposition of $[Mo(CO)_3(Py_3S_3)]$ (1) on Au(111) surfaces and investigation by IRRAS

After characterization of the carbonyl complex **1** in solution and the solid state, complex **1** was also deposited on Au(111) surfaces (for more details see ESI Chapter 1†). The resulting monolayers were investigated by Polarisation–Modulation infrared reflection absorption spectroscopy (PM-IRRAS). The IRRA spectrum of $[Mo(CO)_3(Py_3S_3)]$ (**1**) absorbed on Au(111) is shown along with the bulk IR and calculated IR and IRRA spectra in Fig. 4. In the IRRA spectrum the intensities of the vibrations are in the range of 10^{-3} absorbance units, indicating the formation of a monolayer.[8,28,29,32,33] Due to the surface selection rule of IRRA spectroscopy,[34] the relative intensities of the bands in the bulk IR and IRRA spectra differ, which can provide accurate information about the orientation of the molecules on the surfaces. For the simulated IRRA spectrum, complex **1** was aligned in such a way that the plane spanned by the three pyridine nitrogen atoms is oriented parallel to the surface (*xy* plane) and without the underlying gold surface (for more details see ESI Chapter 9.2†).

The experimental and calculated bulk IR spectra of complex **1** look very similar to each other (see Fig. 4) Consequently, the bands appearing in the measured spectrum can be assigned to

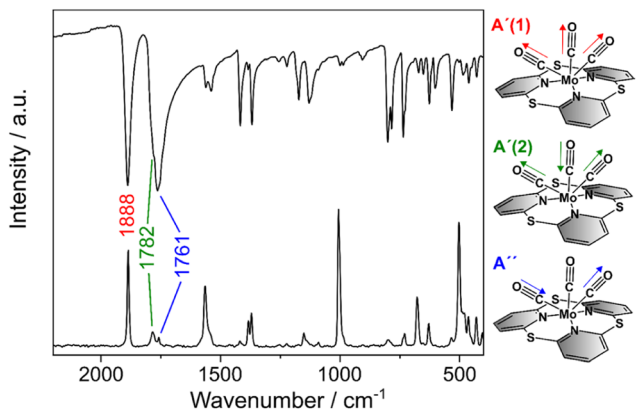

Fig. 3 IR (top) and Raman (bottom) spectra of $[Mo(CO)_3(Py_3S_3)]$ (**1**) between 2200 cm^{-1} and 400 cm^{-1}. The Raman data were multiplied with the factor of 30.

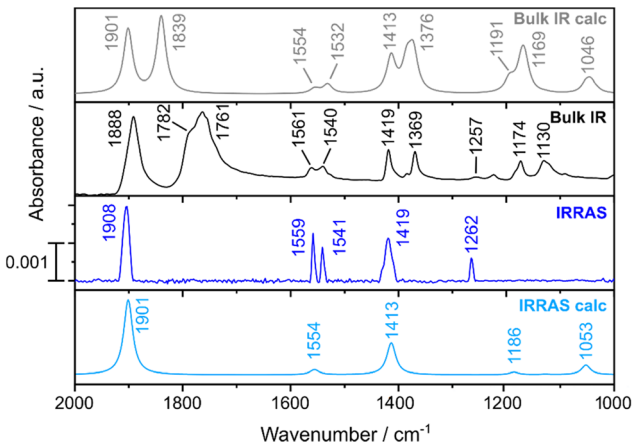

Fig. 4 Calculated and measured vibrational spectra of $[Mo(CO)_3(Py_3S_3)]$ (**1**) in bulk material and adsorbed on Au(111) surfaces.

specific vibrational modes (*cf.* ESI Table S2†). The most prominent bands in the bulk IR spectrum are the three stretching vibrations of the carbonyl ligands. The calculated spectrum exhibits in this region only two discernible vibrational modes. This phenomenon can be attributed to the fact that the A′(1) and A″ vibrations are in such close proximity within the calculation that they appear as a single band (for further details, please refer to Table S2†). The remaining absorption bands of the bulk IR spectrum are attributed to the thiacalixpyridine ligand and can be assigned as C=C stretching vibrations (1561 cm^{-1}, 1540 cm^{-1}, 1419 cm^{-1}), C=N=C stretching vibration (1369 cm^{-1}) and C–H bending modes (1174 cm^{-1}, 1130 cm^{-1}), respectively.

In the experimental IRRA spectrum the totally symmetric A′(1) mode is located at 1908 cm^{-1}. The other two vibrations are not observable (Fig. 4). This means that the transition dipole moments (TDM) of the A′(2) and A″ stretching vibrations are oriented in the *xy* plane and, due to the surface selection rule, no intensity results in the spectrum (for more details see ESI Chapter 4.2†). Compared to the bulk IR spectrum other differences can be identified: three absorption bands of the ligand at 1369 cm^{-1}, 1174 cm^{-1} and 1130 cm^{-1} are missing as well, and the absorption band at 1262 cm^{-1} is more intense.

While a parallel orientation of the complex can be inferred from the fact that only the totally symmetric component A′(1) of the CO stretches is observed, the appearance of two other bands is not consistent with this picture. Specifically, of the four bands observed between 1250 cm^{-1} and 1600 cm^{-1} in the IRRAS, only two should be visible: the characteristic C=C stretching vibrations of the ligand at 1559 cm^{-1} and 1419 cm^{-1} (*cf.* Fig. 4). The other two vibrations at 1541 cm^{-1} and 1262 cm^{-1} have no intensity in the simulated IRRA spectrum. This discrepancy might be due to the fact that the calculation was done without the underlying gold surface. However, the adsorbed complex molecules interact with the surface, which may result in a change of the TDM components of certain vibrational modes along the *z*-axis. Direct interaction of the pyridine rings with the underlying metal atoms could also lead to different vibrational modes compared to the gas phase. In any case, the two bands at 1541 cm^{-1} and 1262 cm^{-1} are observed for two copper(I) complexes supported by thiacalixpyridine ligand **2** and adsorbed to Au(111) as well, demonstrating that these bands are in fact characteristic for such systems deposited on gold surfaces (see ESI Chapter 4.1†).

An interesting aspect in the IRRA spectra of surface-adsorbed Mo(0) carbonyl complexes is the shift of the CO stretching vibrations relative to the crystalline solid, caused by the electronic influence of the metallic substrate. On Au(111), the vibrations are always found to be shifted to higher wavenumber with regard to the bulk, reflecting an overall transfer of electron density from the Mo(0) complex to the surface ("static (de)activation"). This phenomenon can be reduced to some degree by another effect: by virtue of this "dynamic activation" charge flows from the metal center into the π* orbitals of the carbonyl ligands when the C–O bonds are elongated. However, this only comes into play for the totally symmetric A′(1) vibration where all CO-ligands move in phase.[8,28,29] Unfortunately, however, these two effects cannot be observed separately for complex **1** as the IRRA spectrum only contains the totally symmetric vibration A′(1), which is shifted by 20 cm^{-1} to higher wavenumbers. The intensities of the other two carbonyl vibrations, which are only influenced by the static deactivation, vanish due the surface selection rule, so that the interplay of both effects cannot be determined. What can be stated, however, is that the (deactivating) shift of the totally symmetric vibration of complex **1** is distinctly (14 cm^{-1}) larger than observed for the previously investigated molybenum(0) tricarbonyl complex supported by an azacalixpyridine ligand.[8] This reflects a stronger influence of the gold surface on the electronic properties of **1** with respect to its azacalixpyridine-supported analogue which in turn can be traced back to a perfectly coplanar adsorption geometry of the former as opposed to a slightly tilted adsorption geometry of the latter complex on the Au(111) surface. In addition, there is evidence for binding of the S-atoms contained in the thiacalixpyridine ligand to the surface, enhancing the interaction of **1** with the gold surface (see below).

Deposition of $[Mo(CO)_3(Py_3S_3)]$ (1) on Ag(111) and Au(111) surfaces and characterization by UHV methods

After characterization of the surface-adsorbed molybdenum(0) tricarbonyl complex **1** with IRRAS, monolayers of this complex were also deposited on Ag(111) and Au(111) by immersing a substrate in to a solution of **1** (XPS and NEXAFS) or by vacuum evaporation (STM) and investigated under UHV conditions with a range of surface-spectroscopic and -analytical methods. These results are described in the following section.

Scanning tunneling microscopy

Submonolayers of $[Mo(CO)_3(Py_3S_3)]$ molecules (**1**) were prepared on Ag(111) and Au(111) surfaces at room temperature and investigated with a scanning tunnelling microscope (STM) at 4.7 K. On Ag(111) (Fig. 5a), the molecules adsorb individually and no aggregation into molecular islands is observed, suggesting that the diffusion of the molecules is inefficient or that the adsorbed molecules repel each other. The constant-current images of the molecule significantly depend on the applied sample voltage. At high sample voltage (*e.g.*, V = 1.5 V, Fig. 5b and d), the molecule is clover shaped with three identical lobes that appear ≈240 pm higher than the metal substrate. At low voltage, the height of the lobes is reduced by ≈120pm (blue arrow in Fig. 5c and d, V = 50 mV). Meanwhile, additional elongated lobes and a central maximum (black and white arrows in Fig. 5c), are observed.

On Au(111), irregular structures (white arrows in Fig. S12†) were observed in addition to intact molecules. Such structures are absent on Ag that was prepared with identical complexes suggesting that some fragmentation occurs on Au(111). The decomposition on gold may be caused by stronger binding of the S atoms to the substrate (see below).[35] However, an increased dispersive interaction may also be involved.[36] The STM data thus indicate $[Mo(CO)_3(Py_3S_3)]$ molecules (**1**) can be

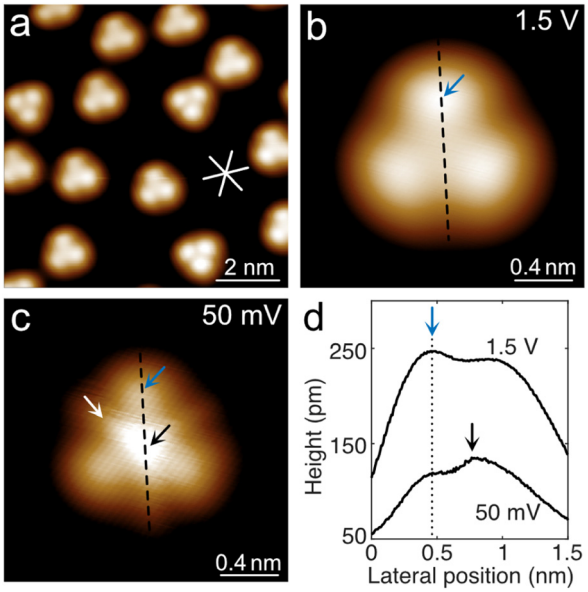

Fig. 5 $[Mo(CO)_3(Py_3S_3)]$ (**1**) on Ag(111). (a) Overview topograph measured at a sample voltage V = 1.5 V and a current I = 30 pA. White lines denote close-packed directions of the (111)-surface. (b) Detailed topograph of a single $[Mo(CO)_3(Py_3S_3)]$ complex (**1**) recorded at 1.5 V and 100 pA. (c) Topograph of the same area recorded at lower voltage (50 mV, 100 pA) and correspondingly reduced tip–molecule distance. A black arrow depicts the new central maximum. A white arrow indicates one of three elongated lobes. The blue arrows in (b) and (c) denote identical lateral positions. The topographs in (b) and (c) have been rotated by 13° with respect to (a). (d) Line profiles measured along the dashed lines in (b) and (c). The black and blue arrows mark the positions defined in panel (c).

deposited intactly on Ag(111) by vacuum evaporation while on Au(111) the integrity of the vacuum-deposited molecules is slightly affected.

X-ray photoelectron spectroscopy

IRRA spectroscopic measurement of the $[Mo(CO)_3(Py_3S_3)]$ (**1**) deposited on Au(111) from solution showed the typical vibrational bands of this complex (see above). In order to further check whether this complex **1** was deposited intactly and without contaminations on gold surfaces X-ray photoelectron spectroscopy (XPS) was employed. To determine the binding energies of the different atomic species located in the S 2p, C 1s, Mo 3d and N 1s spectra, the different spectral regions were measured with acquisition times of up to one hour.

The XP spectra of **1** are presented in Fig. 6. The major signals shown in the survey spectrum (Fig. S14†) are the Au 4f lines at 84.0 eV and 87.5 eV. Futhermore, the Au 4d signals at 335.0 eV and 352.5 eV are clearly visible as well as the C 1s peak at 284.5 eV. The ratio of the Au $4d_{5/2}$ signal to the C 1s signal reveals the presence of a monolayer of the molybdenum complex **1**.[8,28,29,33,37]

The Mo 3d XP spectrum (Fig. 6a) contains a total of three different species each of which exhibits a doublet with an

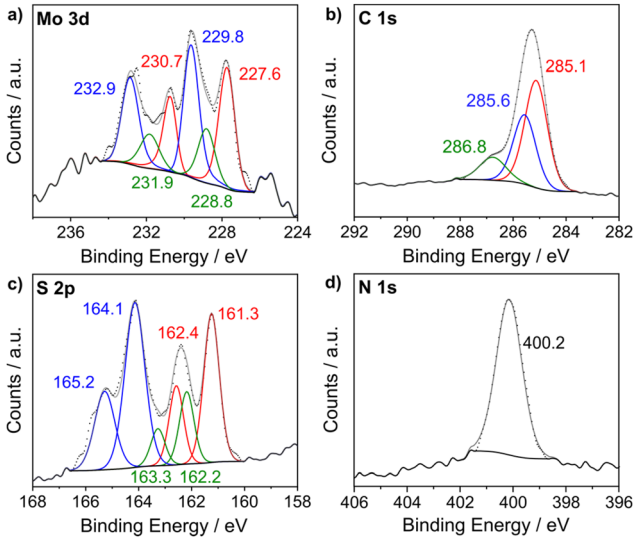

Fig. 6 Mo 3d (a), C 1s (b), S 2p (c) and N 1s (d) XP spectra of a monolayer of $[Mo(CO)_3(Py_3S_3)]$ (**1**) on Au(111).

intensity ratio of 3 : 2 and the typical splitting of 3.0–3.1 eV.[8,28,29] The species with the lowest binding energy of 227.6 eV and 230.7 eV (red) can be assigned to molybdenum(0) and corresponds to the intact complex **1**. The two other doublets (228.8 eV and 231.9 eV green; 229.8 and 232.9 eV blue) are associated with cationic molybdenum species, presumably in oxidation states of +2 (green) and +4 (blue; see Fig. 6a), respectively.[38] This would be similar to the molybdenum(0) tricarbonyl complex supported by an azacalix[3]pyridine ligand which we studied previously.[8] However, whereas complete conversion to a Mo(VI) oxo complex was observed for the latter system, the fully oxidized Mo(VI) species is not found in the case of **1**. For this complex, an intensity ratio of Mo(0) : Mo(II) : Mo(IV) is 37 : 19 : 44 is observed. Overall, these data reflect a higher stability of **1** towards oxidation as compared to its azacalix[3]pyridine-supported analogue studied before.[8] We assume that this is due to the larger ring size of the thia- as compared to the azacalixpyridine ligand, allowing a more regular (*i.e.*, less trigonally distorted) octahedral coordination of the Mo(0) central atom (see above).

The C 1s spectrum shows three signals (Fig. 6b). The most prominent signal at 285.1 eV (red trace) reflects the carbon atoms which are bonded to other carbon atoms. The second species (blue line) at 285.6 eV belongs to carbon atoms bound to heteroatoms (C–N). The third species (green) is assigned to carbon atoms bonded to highly electronegative elements, in this case to oxygen.[29] The areas of the three signals yield a ratio of 53 : 35 : 12. The proportion of the thiacalixpyridine ligand is higher and for the carbonyl ligands lower than the theoretical ratio 50 : 33 : 17. This shows that some of the CO ligands have dissociated from the surface-deposited molecules of **1**, which is compatible with the observation from the Mo 3d spectrum that a part of the complexes have been oxidized to Mo(II) and Mo(IV) (Fig. 6a).

The S 2p spectrum (Fig. 6c) contains three species, each of which has an intensity ratio of 2 : 1 and the typical spin–orbit splitting of 1.1–1.2 eV.[39–42] The main signal at 164.1 eV and 165.2 eV (blue lines) can be assigned to the bridging sulfur atoms of **1** (see also Fig. S16a†), which are located above the level of the bridged carbon atoms of the pyridines (see Fig. 2). In this geometry, the two lone pairs of the sp^3-hybridized sulfur atoms cannot interact with the underlying gold atoms (see Fig. S17†). However, if a thioether bridge is flipped downwards, one of the sulfur lone pairs can bind to the Au(111) surface (see Fig. S17†). The green trace doublet at 162.2 eV and 163.3 eV may belong to this typical sulfur species bound to gold.[39,40,42,43]

At lower energies at 161.3 eV and 162.4 eV (red) a third species appears, which is generally observed in thiol-derived SAMS on Au substrates.[42,44] In the literature, it is usually assigned to adsorbed sulfur atoms[45] or a differently adsorbed organothiol species on gold. The first possibility could reflect a decomposition of the molecules on the Au surface, forming chemisorbed sulfur. This would be compatible with the STM results and indicate that a fraction of the molecules decomposes when deposited on this substrate (see above). The second possibility, a differently adsorbed thiol (sulfur) species in the monolayers of complex **1** on Au(111), appears less likely as IRRAS indicates a high degree of molecular orientation in these layers.

The N 1s spectrum (Fig. 6d), finally, only contains one signal at 400.2 eV, which is straightforwardly to the pyridine nitrogen atoms.[8,28] Referring to the XP spectra of all elements of **1** in a "thick" layer (*i.e.*, more than a monolayer; see ESI Chapter 6†), we can conclude that complex **1** is deposited predominantly intactly on a gold surfaces. However, due to the high energy radiation of the synchrotron beam a partial release of carbonyl ligands occurs, leading to a partial oxidation of the molybdenum centers. Nevertheless, the thiacalixpyridine ligand seems to be intact, still coordinating the molybdenum atom.

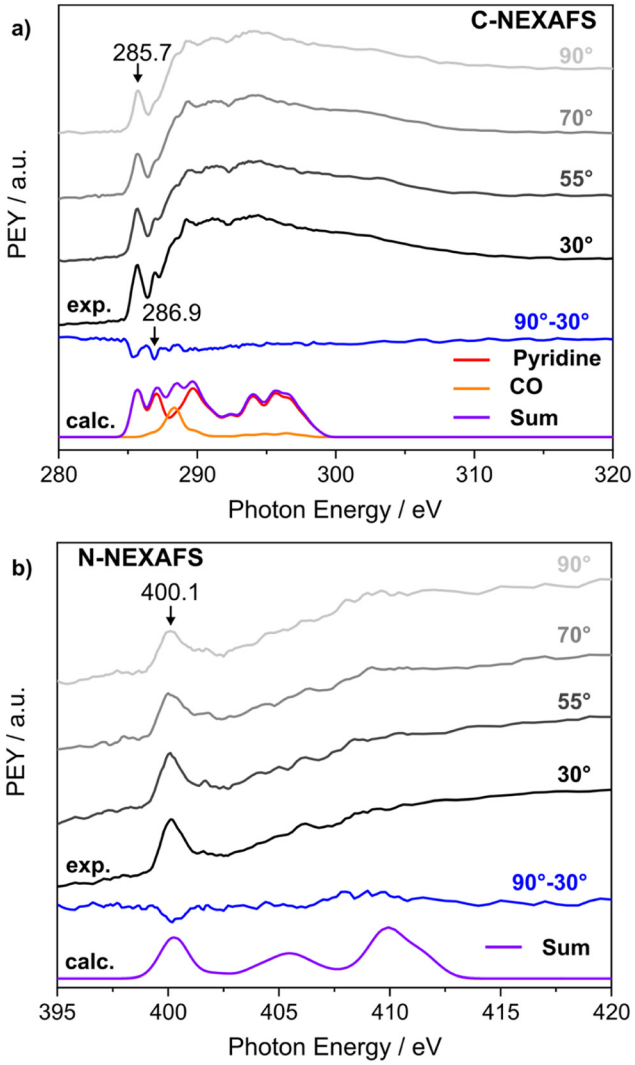

Fig. 7 Normalized NEXAFS spectra of a monolayer of $[Mo(CO)_3(Py_3S_3)]$ (**1**) on Au(111) at different angles (30°, 55°, 70°, 90°) and the calculated NEXAFS data (shifted by +11.4 eV (C) and +13.3 eV (N)) with the contribution of the different subunits summed over all angles: (a) C K-edge spectrum; (b) N K-edge spectrum.

Near-edge X-ray absorption fine structure

Besides providing electronic structural information, near-edge X-ray absorption fine structure (NEXAFS) is well suited to determine the orientation of molecules adsorbed on surfaces. With this in mind NEXAFS measurements were performed for monolayers of the $[Mo(CO)_3(Py3S_3)]$ (**1**) on Au(111) single crystals at the C and N K-edge, employing different angles of incidence (Fig. 7).

The C K-edge spectrum, shown in Fig. 7a, exhibits two π* resonances located at 285.7 eV and 286.9 eV which also can be found in the spectrum derived from DFT calculations (Fig. 7a, bottom). Both resonances are assigned to a C 1s to π* transition of the pyridine moiety.[8,28] With increasing angle of incidence, the intensities of both resonances slightly decrease. The N K-edge spectrum shows one intense π* resonance at 400.1 eV, which can be assigned to the N 1s to LUMO transition of the pyridine nitrogen atoms (see Fig. 7b).[8,28] The intensity of this signal also slightly decreases with increasing angle of incidence.

As shown in the IRRA-spectroscopic investigation (see above) the basal plane of the $[Mo(CO)_3(py)_3]$ complex has a parallel orientation to the surface. Using the angles from the crystal structure the out-of-plane p-orbitals of the pyridine C and N atoms have angles of α = 46–48° to the surface normal (see Fig. S18†). This is close to the magic angle (54.7°), which means that only a small angular dependence is expected for the two C 1s to π* and the N 1s to π* transition of the pyridine C and N atoms, in agreement with the experimental spectra.[46,47] Nevertheless, the observed (small) angular dependence allows determination of α using eqn (1) which describes the relationship between the intensity I of the resonant transition, the angle α of the transition dipole moment (TDM), the

incidence angle of the radiation θ and the polarization P of the incident X-ray light:[46–48]

$$I \propto P\cdot\cos^2(\theta)\cdot(1 - 1.5\cdot\sin^2(\alpha)) + 0.5\cdot\sin^2(\alpha) \quad (1)$$

Using the intensities of the isolated resonances at 285.7 eV (C 1s – π*) and 400.1 eV (N 1s – π*) at different angles of incidence θ and applying formula (1), the angle α of the transition dipole moments for the two transitions mentioned above (which are assumed to be collinear) can be determined. As evident from Fig. S19,† we obtained an angle α of 48 ± 2°, which fits very well to the orientation of the pyridine rings based on the crystal structure along with an orientation of the molecules parallel to the surface. This means that the interaction with the gold surface neither causes a flattening nor a steepening of the trigonal-pyramidal Mo–N(pyridine)$_3$ unit of **1** compared to the crystal structure.

According to the calculation, a π* transition is expected at 288.4 eV for the carbonyl C atoms of **1**. However, no distinct resonance can be identified at this position and no significant feature is seen in the difference spectrum either (see Fig. 7a, blue spectrum). In any case, the carbonyl C atoms would also only have a small angular dependence as the carbonyl π-orbitals have an angle γ of 47–49° with respect to the surface normal (see Fig. S18†) when modelled according to the same criteria as above. Overall, the NEXAFS data thus confirms the parallel orientation complex **1** with respect to the metallic surface.

Reactivity towards oxygen (O_2)

By reaction with molecular oxygen, the previously investigated molybdenum(0) tricarbonyl complex supported by an azacalixpyridine ligand showed a conversion to a Mo(VI) trioxo complex within one hour in homogeneous solution.[9] This reactivity could be observed for the azacalixpyridine complex deposited on a Au(111) surface as well.[9] Due to the similarity of the supporting ligands, we wanted to know whether the thiacalixpyridine complex **1** also undergoes oxygenation under comparable conditions. However, this complex turned out to be stable in solution under oxygen atmosphere over hours. After a few days, the color of the solution gradually changed from red to grey. Obviously, a demetalation process occurred, producing a grey colored precipitate, which we could not identify, whereby the free ligand **2** could be recovered from the solution. The reactivity of complex **1** towards oxygen was investigated as well when deposited on a Au(111) surface. Under oxygen atmosphere and irradiation with 365 nm a photodissociation of the CO ligands could be observed, similar to the azacalixpyridine complex. However, compared to the latter the half-life for the photodissociation was 10 times longer (for more details see ESI Chapter 8†).

To understand why complex **1** does not react to the hypothetical molybdenum(VI) trioxo complex **3** in analogy to the previously reported azacalixpyridine system[9] (see Scheme 2), DFT calculations were performed.

The structure of the hypothetical molybdenum(VI) trioxo complex **3** was successfully optimized (see Fig. S24† right). It exhibits O–Mo–O angle of 108°, which is in the typical range for MoO_3 complexes (105–108°).[20,49] However, with 2.425 Å the Mo–N bond length is drastically increased with respect to the carbonyl complex **1** as well as the molybdenum complexes supported by the azacalixpyridine ligand (see Table 2). During the hypothetical conversion of **1** to **3** the average N–Mo–N bond angles changes over 8°, which results in a highly distorted octahedral geometry. With 72.19° the N–Mo–N angle and the Mayer bond order (0.2671) of the Mo–N bonds of **3** are approximately the same as in the azacalixpyridine complexes. However, the Mo–N Mayer bond order of the hypothetical oxo complex **3** decreases dramatically compared to the value of the carbonyl complex **1** (*cf.* Table 2). This shows that the almost regular octahedral structure in **1** is significantly more stable than the highly distorted geometry in the oxo complex **3**, thus preventing the conversion shown in Scheme 2. Furthermore, the DFT calculations demonstrate that this hypothetical reaction is highly endergonic (+1110 kcal mol^{-1}), whereas calculation of the analogous reaction of the azacalixpyridine system gives a negative free reaction energy (−172.5 kcal mol^{-1}).[9]

Replacing the bridging tolylamine groups by sulfur atoms thus increases the size of the cavity of the supporting ligand and enables a more regular octahedral coordination of the Mo(0) center in **1** compared to its azacalixpyridine supported analog.[9] On the other hand, it acts to reduce the reactivity towards molecular oxygen, both in solution and on the surface, whereby in both cases the exact identity of the reaction product is unknown.

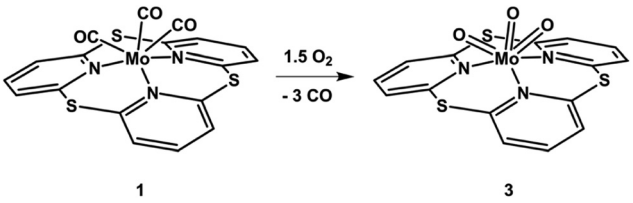

1 3

Scheme 2 Hypothetical conversion of the carbonyl complex 1 with molecular oxygen into the molybdenum(VI) trioxo complex [$MoO_3(Py_3S_3)$] (**3**).

Table 2 Bond lengths, angles and Mayer bond orders of the Mo–N bonds of the thiacalixpyridine supported carbonyl **1** and oxo **3** complexes and for the azacalix-pyridine analogs

	Bond length, Mo–N/Å	Bond angle, N–Mo–N/°	Mayer bond order, Mo–N
[$Mo(CO)_3(Py_3S_3)$] (**1**)[a]	2.277	80.92	0.7485
[$MoO_3(Py_3S_3)$] (**3**)[b]	2.425	72.90	0.2671
[$Mo(CO)_3$(Tolyl-ACP)][c]	2.249	72.19	0.3085
[MoO_3(Tolyl-ACP)][c]	2.319	68.75	0.3068

[a] This study. [b] PBE0/TZVP computional results in the gas phase. [c] Values from ref. 8 and 9.

Conclusions

In order to explore a new approach to activate small molecules by deposition of dome-shaped metal organic complexes

(MOCs) on metallic surfaces, a molybdenum(0) tricarbonyl complex (**1**) supported by a tridentate thiacalix[3]pyridine has been synthesized and adsorbed on noble metallic surfaces. Monolayers of **1** on Ag(111) or Au(111) were investigated using different surface-spectroscopic and -analytical methods (IRRAS, STM, XPS, NEXAFS). Whereas the intact complex could be measured under STM and IRRAS conditions, the vacuum evaporated complex loses some of the CO ligands by X-ray irradiation in the XPS and (partly) oxidized molybdenum species can be detected. The NEXAFS and IRRAS measurements demonstrate a parallel orientation of the dome-shaped complex **1** with respect to the surface. Due to this orientation of the molybdenum(0) tricarbonyl headgroup only the totally symmetric A′(1) vibrational mode of the molybdenum(0) tricarbonyl headgroup is detectable in the IRRA spectrum and the A′(2)/A″ vibrations vanish in intensity due to the surface selection rule. Nevertheless, a strong influence of the underlying gold substrate on the activation of the carbonyl ligands is observed.

Overall, replacing the bridging tolylamine groups in the azacalixpyridine ligand by sulfur atoms improves the adsorption geometry such that an exactly coplanar orientation of the derived molybdenum(0) tricarbonyl complex (**1**) with respect to a metallic surface is now obtained. Using bridging thioethers expands the ring size (cavity) of the ligand and thus leads to a more regular octahedral coordination. This increases the stability of **1** towards molecular oxygen but may also reduce the catalytic activity of the corresponding metal surface/metalorganic complex (MOC) hybrid system with respect to its azacalixpyridine analog.[8,9]

Data availability

The spectral data supporting this article are available in the ESI† of this article.

Crystallographic data for compound **1** has been deposited at the CCDC under [CCDC 2366199] and can be obtained from **https://www.ccdc.cam.ac.uk/strucutres**.

Conflicts of interest

There are no conflicts to declare.

Acknowledgements

The authors would like to thank the HZB for provision of beamtime at the BESSYII/HE-SGM (XPS and NEXAFS measurements) and Christof Wöll/KIT and the BAM/Berlin for the provision of the Prevac endstation. The authors thank Alexei Nefedov for using the transfer box of the HE-SGM beamline. Finally, the authors would like to thank Tobias A. Engesser for help with spectroscopic measurements.

References

1 W. Grünert, W. Kleist and M. Muhler, *Catalysis at Surfaces*, De Gruyter, Berlin Germany, Boston MA, 2nd edn, 2023.
2 (*a*) J. Hagen, *Industrial catalysis. A practical approach*, John Wiley & Sons, 2015; (*b*) S. K. Kaiser, Z. Chen, D. Faust Akl, S. Mitchell and J. Pérez-Ramírez, *Chem. Rev.*, 2020, **120**, 11703–11809.
3 C. Copéret, M. Chabanas, R. P. Saint-Arroman and J.-M. Basset, *Angew. Chem., Int. Ed.*, 2003, **42**, 156–181.
4 C. Copéret, A. Comas-Vives, M. P. Conley, D. P. Estes, A. Fedorov, V. Mougel, H. Nagae, F. Núñez-Zarur and P. A. Zhizhko, *Chem. Rev.*, 2016, **116**, 323–421.
5 M. K. Samantaray, V. D'Elia, E. Pump, L. Falivene, M. Harb, S. Ould-Chikh, L. Cavallo and J.-M. Basset, *Chem. Rev.*, 2020, **120**, 734–813.
6 M. K. Samantaray, E. Pump, A. Bendjeriou-Sedjerari, V. D'Elia, J. D. A. Pelletier, M. Guidotti, R. Psaro and J.-M. Basset, *Chem. Soc. Rev.*, 2018, **47**, 8403–8437.
7 J. D. A. Pelletier and J.-M. Basset, *Acc. Chem. Res.*, 2016, **49**, 664–677.
8 K. U. Clausen, A. Schlimm, K. Bedbur, C. Näther, T. Strunskus, L. Fu, M. Gruber, R. Berndt and F. Tuczek, *Chem. – Eur. J.*, 2024, **30**, e202303912.
9 K. U. Clausen, N. Pienack, J. Gripp and F. Tuczek, *Chem. – Eur. J.*, 2024, **30**, e202304359.
10 X. Meng, M. L. Nguyen, A. Weismann, C. Li, F. Tuczek and R. Berndt, *J. Phys. Chem. C*, 2023, **127**, 12118–12124.
11 K. Flechtner, A. Kretschmann, H.-P. Steinrück and J. M. Gottfried, *J. Am. Chem. Soc.*, 2007, **129**, 12110–12111.
12 J. M. Gottfried, *Surf. Sci. Rep.*, 2015, **70**, 259–379.
13 M. DeJong, A. J. A. Price, E. Mårsell, G. Tom, G. D. Nguyen, E. R. Johnson and S. A. Burke, *Nat. Commun.*, 2022, **13**, 7407.
14 (*a*) *Handbook of Porphyrin Science (Volume 16)*, ed. K. M. Kadish, K. M. Smith and R. Guilard, World Scientific Publishing Company, 2012, vol. 20; (*b*) I. Hod, M. D. Sampson, P. Deria, C. P. Kubiak, O. K. Farha and J. T. Hupp, *ACS Catal.*, 2015, **5**, 6302–6309; (*c*) P. Gotico, B. Boitrel, R. Guillot, M. Sircoglou, A. Quaranta, Z. Halime, W. Leibl and A. Aukauloo, *Angew. Chem., Int. Ed.*, 2019, **58**, 4504–4509; (*d*) Y. Hu, K. Lang, J. Tao, M. K. Marshall, Q. Cheng, X. Cui, L. Wojtas and X. P. Zhang, *Angew. Chem., Int. Ed.*, 2019, **58**, 2670–2674.
15 W. Hieringer, K. Flechtner, A. Kretschmann, K. Seufert, W. Auwärter, J. V. Barth, A. Görling, H.-P. Steinrück and J. M. Gottfried, *J. Am. Chem. Soc.*, 2011, **133**, 6206–6222.
16 (*a*) S. Shimizu, *Chem. Rev.*, 2017, **117**, 2730–2784; (*b*) S. Shimizu, *Angew. Chem., Int. Ed.*, 2023, **62**, e202217099; (*c*) D. Kuzuhara, H. Yamada, Z. Xue, T. Okujima, S. Mori, Z. Shen and H. Uno, *Chem. Commun.*, 2011, **47**, 722–724; (*d*) D. Prasannan and M. Ravikanth, *Coord. Chem. Rev.*, 2020, **407**, 213172.
17 (*a*) J. G. Serafin, A. C. Liu and S. R. Seyedmonir, *J. Mol. Catal. A: Chem.*, 1998, **131**, 157–168; (*b*) M. M. Montemore, M. A. van Spronsen, R. J. Madix and C. M. Friend, *Chem. Rev.*, 2018, **118**, 2816–2862; (*c*) X. Liu, R. J. Madix and

C. M. Friend, *Chem. Soc. Rev.*, 2008, **37**, 2243–2261; (*d*) W. Huang, G. Sun and T. Cao, *Chem. Soc. Rev.*, 2017, **46**, 1977–2000; (*e*) T. V. Choudhary, S. Banerjee and V. R. Choudhary, *Appl. Catal., A*, 2002, **234**, 1–23; (*f*) E. Carter and W. Goddard III, *J. Catal.*, 1988, **112**, 80–92; (*g*) C. Schröder, M. C. Schmidt, P. A. Haugg, A.-K. Baumann, J. Smyczek and S. Schauermann, *Angew. Chem., Int. Ed.*, 2021, **60**, 16349–16354; (*h*) S. Attia, M. C. Schmidt, C. Schröder and S. Schauermann, *ACS Catal.*, 2019, **9**, 6882–6889; (*i*) M. Lackinger, *Chem. Commun.*, 2017, **53**, 7872–7885; (*j*) G. Galeotti, M. Fritton and M. Lackinger, *Angew. Chem., Int. Ed.*, 2020, **59**, 22785–22789.

18 Y. Suzuki, T. Yanagi, T. Kanbara and T. Yamamoto, *Synlett*, 2005, 263–266.

19 R. Tanaka, T. Yano, T. Nishioka, K. Nakajo, B. K. Breedlove, K. Kimura, I. Kinoshita and K. Isobe, *Chem. Commun.*, 2002, 1686–1687.

20 L. Xu, Y. Sasaki and M. Abe, *Chem. Lett.*, 1999, **28**, 163–164.

21 A. J. Plajer, A. L. Colebatch, M. Enders, Á. García-Romero, A. D. Bond, R. García-Rodríguez and D. S. Wright, *Dalton Trans.*, 2018, **47**, 7036–7043.

22 C.-Y. Kuo, Y.-S. Fuh, J.-Y. Shiue, S. J. Yu, G.-H. Lee and S.-M. Peng, *J. Organomet. Chem.*, 1999, **588**, 260–267.

23 H. Kelm and H.-J. Krüger, *Eur. J. Inorg. Chem.*, 1998, **1998**, 1381–1385.

24 N. L. Armanasco, M. V. Baker, M. R. North, B. W. Skelton and A. H. White, *J. Chem. Soc., Dalton Trans.*, 1998, 1145–1150.

25 M. V. Baker, D. H. Brown, B. W. Skelton and A. H. White, *J. Chem. Soc., Dalton Trans.*, 2000, 4607–4616.

26 C.-X. Zhang, D.-W. Fang, J.-L. Wang, A.-Q. Jia and Q.-F. Zhang, *Inorg. Chim. Acta*, 2020, **507**, 119599.

27 S. P. van Kouwenberg, E. H. Wong, G. R. Weisman, E. J. Gabe, F. L. Lee and P. Jackson, *Polyhedron*, 1989, **8**, 2333–2338.

28 A. Schlimm, N. Stucke, B. M. Flöser, T. Rusch, J. Krahmer, C. Näther, T. Strunskus, O. M. Magnussen and F. Tuczek, *Chem. – Eur. J.*, 2018, **24**, 10732–10744.

29 F. Petersen, I. Lautenschläger, A. Schlimm, B. M. Flöser, H. Jacob, R. Amirbeigiarab, T. R. Rusch, T. Strunskus, O. Magnussen and F. Tuczek, *Dalton Trans.*, 2021, **50**, 1042–1052.

30 (*a*) J. Weidlein, U. Mueller and K. Dehnicke, *Schwingungsspektroskopie*, Thieme, Stuttgart usw., 1982; (*b*) K. Nakamoto, *Infrared and Raman Spectra of Inorganic and Coordination Compounds*, Wiley, Hoboken, 2008.

31 H. Vu, M. R. Atwood and B. Vodar, *J. Chem. Phys.*, 1963, **38**, 2671–2677.

32 C. J. Miller, F. M. Brunner, H. R. Kelly, P. L. Cheung, N. A. Torquato, M. Gembicky, S. Okuno, T. Chan, V. S. Batista and C. P. Kubiak, *Dalton Trans.*, 2022, **51**, 17688–17699.

33 H. Jacob, S. Ulrich, U. Jung, S. Lemke, T. Rusch, C. Schütt, F. Petersen, T. Strunskus, O. Magnussen, R. Herges and F. Tuczek, *Phys. Chem. Chem. Phys.*, 2014, **16**, 22643–22650.

34 R. G. Greenler, *J. Chem. Phys.*, 1966, **44**, 310–315.

35 A. H. Pakiari and Z. Jamshidi, *J. Phys. Chem. A*, 2010, **114**, 9212–9221.

36 S. Johannsen, M. Gruber, C. Barreteau, M. Seredyuk, J. A. Real, T. Markussen and R. Berndt, *J. Phys. Chem. Lett.*, 2023, **14**, 7814–7823.

37 A. Schlimm, R. Löw, T. Rusch, F. Röhricht, T. Strunskus, T. Tellkamp, F. Sönnichsen, U. Manthe, O. Magnussen, F. Tuczek and R. Herges, *Angew. Chem.*, 2019, **131**, 6646–6650.

38 (*a*) J. Brisdon, W. S. Mialki and R. A. Walton, *J. Organomet. Chem.*, 1980, **187**, 341–347; (*b*) D. O. Scanlon, G. W. Watson, D. J. Payne, G. R. Atkinson, R. G. Egdell and D. S. L. Law, *J. Phys. Chem. C*, 2010, **114**, 4636–4645; (*c*) J. Baltrusaitis, B. Mendoza-Sanchez, V. Fernandez, R. Veenstra, N. Dukstiene, A. Roberts and N. Fairley, *Appl. Surf. Sci.*, 2015, **326**, 151–161.

39 E. Fast, A. Schlimm, I. Lautenschläger, K. U. Clausen, T. Strunskus, C. Spormann, T. K. Lindhorst and F. Tuczek, *Chem. – Eur. J.*, 2020, **26**, 485–501.

40 H. Jacob, K. Kathirvel, F. Petersen, T. Strunskus, A. Bannwarth, S. Meyer and F. Tuczek, *Langmuir*, 2013, **29**, 8534–8543.

41 M. E. Fleet, S. L. Harmer, X. Liu and H. W. Nesbitt, *Surf. Sci.*, 2005, **584**, 133–145.

42 A. Shaporenko, A. Terfort, M. Grunze and M. Zharnikov, *J. Electron Spectrosc. Relat. Phenom.*, 2006, **151**, 45–51.

43 (*a*) C. Silien, M. Buck, G. Goretzki, D. Lahaye, N. R. Champness, T. Weidner and M. Zharnikov, *Langmuir*, 2009, **25**, 959–967; (*b*) S. Frey, H.-T. Rong, K. Heister, Y.-J. Yang, M. Buck and M. Zharnikov, *Langmuir*, 2002, **18**, 3142–3150.

44 (*a*) T. Weidner, N. Ballav, U. Siemeling, D. Troegel, T. Walter, R. Tacke, D. G. Castner and M. Zharnikov, *J. Phys. Chem. C*, 2009, **113**, 19609–19617; (*b*) T. Weidner, A. Krämer, C. Bruhn, M. Zharnikov, A. Shaporenko, U. Siemeling and F. Träger, *Dalton Trans.*, 2006, 2767–2777; (*c*) M. Zharnikov, *J. Electron Spectrosc. Relat. Phenom.*, 2010, **178–179**, 380–393.

45 (*a*) Y. Liu, S. Katzbach, A. Asyuda, S. Das, A. Terfort and M. Zharnikov, *Phys. Chem. Chem. Phys.*, 2022, **24**, 27693–27704; (*b*) C. Vericat, M. E. Vela, G. Benitez, P. Carro and R. C. Salvarezza, *Chem. Soc. Rev.*, 2010, **39**, 1805–1834.

46 J. Stöhr, *NEXAFS spectroscopy*, Springer Science & Business Media, 2013.

47 J. Stöhr and D. A. Outka, *Phys. Rev. B: Condens. Matter Mater. Phys.*, 1987, **36**, 7891–7905.

48 A. Nefedov and C. Wöll, in *Surface Science Techniques*, ed. G. Bracco and B. Holst, Springer Berlin Heidelberg, Berlin, Heidelberg, 2013, pp. 277–303.

49 (*a*) M. V. Baker, M. R. North, B. W. Skelton and A. H. White, *Inorg. Chem.*, 1999, **38**, 4515–4521; (*b*) H. Guo, C. Gong, X. Zeng, H. Xu, Q. Zeng, J. Zhang and J. Xie, *Dalton Trans.*, 2019, **48**, 5541–5550; (*c*) G. Haselhorst, S. Stoetzel, A. Strassburger, W. Walz, K. Wieghardt and B. Nuber, *J. Chem. Soc., Dalton Trans.*, 1993, 83; (*d*) P. C. McGowan, T. J. Podesta and M. Thornton-Pett, *Inorg. Chem.*, 2001, **40**, 1445–1453.

